

# Design of variable stiffness composites for maximum fundamental frequency considering manufacturing constraints of tow steering

Ali Rashed<sup>a,b</sup>, Eralp Demir<sup>c,\*</sup>

<sup>a</sup>*Faculty of Engineering and Natural Sciences, Sabanci University, Tuzla, Istanbul, Turkey*

<sup>b</sup>*Integrated Manufacturing Technology Research and Application Center, Sabanci University, Tuzla, Istanbul, Turkey*

<sup>c</sup>*Department of Mechanical Engineering, University of Bristol, Bristol, BS8 1TR, UK.*

---

## Abstract

In this study, an in-house finite element approach is developed to optimize fundamental frequency of variable stiffness composites considering manufacturing constraints of tow steering process. The method uses the lamination parameters as the design variables. Tow angles or fiber angles and their stacking sequence are computed from the optimum lamination parameters by direct search method. The Least-Squares and Continuity (LSC) method is applied to maintain the fiber or tow continuity within a prescribed curvature limit for manufacturability. Finally the discrete fiber angles or tow directions were converted into paths by using stream functions to have continuous manufacturable paths. The results of the method were compared to various literature findings for constant, balanced variable, and general variable stiffness designs for different boundary conditions, aspect ratios, and material properties. The optimum lamination parameter distributions were in good agreement with literature findings. The maximum fundamental frequency improvements of 11.9 % and 10.2 % were computed by the LSC method with respect to the optimum constant stiffness results for fully simply-supported and fully clamped cases, respectively.

### *Keywords:*

Automated fiber placement, variable stiffness composites, least squares FEM, lamination parameters, optimization, natural frequency

---

## Nomenclature

- [A] coefficient matrix for stream function analysis
- [B] moment-curvature coupling
- [C] global continuity constraint

---

\*Corresponding author

Email address: [eralp.demir@bristol.ac.uk](mailto:eralp.demir@bristol.ac.uk) (Eralp Demir)

$[\mathbf{C}_{el}]$	elemental continuity constraint
$[\mathbf{D}]$	bending stiffness matrix of composite laminate
$[\mathbf{K}]$	global bending stiffness matrix
$[\mathbf{L}]$	global least-squares constraint
$[\mathbf{M}]$	global mass matrix
$[\mathbf{U}]$	material invariant matrix
$\alpha$	penalty factor for continuity constraint
$\kappa_{el}$	elemental curvature
$\kappa_{max}$	maximum elemental curvature limit
$\lambda_i$	eigenvalue of $i$ th mode shape
$\mathbf{x}$	position vector
$\Omega$	domain of analysis
$\omega$	domain of an element
$\bar{f}_1, \tilde{f}_1$	optimum non-dimensional frequency
$\Psi$	stream function
$\theta(\mathbf{x})$	fiber angle as a field variable
$\theta_{opt}$	optimum fiber angles
$\varrho$	material density
$\xi_1, \xi_2, \xi_3, \xi_4$	lamination parameters for bending
$\{\boldsymbol{\Theta}\}$	input vector consisting of given angles for stream function analysis
$\{\boldsymbol{\theta}\}$	global node values of fiber angles
$\{\boldsymbol{\theta}_{el}\}$	elemental node values of fiber angles
$\{\boldsymbol{\xi}\}$	lamination parameter vector for bending stiffness
$\{\mathbf{a}_i\}$	eigenvector of $i$ th frequency
$\{\mathbf{d}\}$	vectorized form of bending stiffness
$\{\mathbf{h}\}$	natural logarithm of thickness function vector (streamline analysis)
$\{\mathbf{N}_\theta\}$	interpolation functions used for LSC

$\{\mathbf{N}\}$	Bogner-Fox-Schmid interpolation functions
$\{\mathbf{q}\}$	global vector of weighted optimum fiber angles
$a$	size of long edge of plate
$b$	size of short edge of plate
$E_{11}, \nu_{12}, \nu_{21}, E_{22}, G_{12}$	lamina elastic constants
$h$	thickness function (streamline analysis)
$Q_{11}, Q_{12}, Q_{22}, Q_{66}$	reduced lamina stiffness constants
$t$	plate thickness
$U_1, U_2, U_3, U_4$	invariant stiffness parameters

## 1. Introduction

Laminated composite materials find applications in different industries such as aerospace, automotive, and naval structures. The high strength to weight ratio of these materials makes them a favorable alternative to conventional metallic alloys for various light-weighting applications. The mechanical strength and stiffness of composite materials are highly dependent on their stacking sequence for constant stiffness (CS) plates; layup angles and layer thicknesses. Current state of the art manufacturing methods, Automated Fiber Placement (AFP), allows steering of tows along the desired directions to manufacture variable stiffness (VS) composites with certain limitations on steering [1, 2]. Therefore, VS composite manufacturing drives for the need of optimization methods to identify tow steering directions and layup sequences to further make the most of composite materials by tailoring composite tows [3, 4].

Various properties of composite structures have been enhanced by optimization methods to compute the fiber angles in layups and their stacking sequence. Natural frequency was one of the objective that was maximized by designing new layup sequence of CS plates [5]. Similarly, fundamental frequency was maximized by considering the effect of the shear stress in the research performed by [6]. More recent studies have focused on improving the compliance of VS composite structures for obtaining the maximum structural rigidity [7, 8, 9]. Furthermore, critical buckling load of VS composites was used as an objective function [10, 11] that revealed over 100% increase in the critical buckling load [12]. Similarly, failure load was enhanced alongside with the frequency response [13].

Maximization of natural frequencies of the composite structures has been an important design criteria for dynamically loaded composite structures. The fundamental frequency of VS composites was optimized by using lamination parameters as the design variable [14], and these parameters were used to compactly represent the directional properties of the composite plates [15]. Similarly, maximizing the fundamental frequency and the damping capacity of tow steered composite panels was performed by [16] in which fiber trajectories were used as the design variables. Accordingly, increasing fundamental frequencies of composite panels of

VS laminates were investigated [17] by considering resulting changes in the relevant mode shapes.

Design optimization methods employed different numerical methods to represent the composite domain. For example, B-splines were used as an efficient way to discretize composites [18, 19]. Apart from that, Bezier curves were used to represent the composite materials [20] which was used to obtain the transient response of the VS composite laminated plates. Similarly, isogeometric methods were used recently to effectively represent composites [19] including NURBS enhanced methods [21].

Various shapes and geometries were studied for VS composite design applications [22, 23, 24]. For example, optimization was used to determine the tow paths for VS cylindrical shell structures that were designed for the AFP process [25]. Likewise, composite plates with elliptical cutouts were investigated for the optimum structural stiffness that also effected the natural frequency of plates [6]. Recently, steering around open-hole tensile geometry was applied to 3D printing process to reduce stress concentrations, that has the same principals as AFP process [26].

Optimization is characterized by the numerical method used as well as design variables, constraints, and objective functions. Previous research studies employed different design variables to maximize the frequency as the objective function. In earlier studies, fiber orientation angles in each of the lamina layers were considered as the design variables [5] that led to non-linear type of optimization. The optimization problem becomes even more challenging for VS applications in which the number of design variables is a multiple of the number of elements, nodes, or knots of the design domain. Therefore, lamination parameters were used as the design variables [7, 14, 8], that converted the optimization into a convex problem with a local minimum. Other design variables such as the parameters of a curved surface were used in minimization of compliance [27]. Similarly, lamination parameters and its application in distance-based interpolation that allowed maximization of the fundamental frequency effectively [15]. Likewise, buckling frequency optimization was performed by using lamination parameters effectively in [28]. In addition, the weight of a composite plate was used as an objective function that was minimized subject to frequency constraints by using the fiber volume fraction and laminate thickness as the design variables [29].

Manufacturability of designs has been the major concern in realizing the optimization findings. Curvature is the major parameter that controls the directional properties; in CS plates tows are parallel with zero curvature while in VS plates tows can be steered with a curvature constraint. Designs based on the manufacturability restrictions were developed for practical applications by keeping the curvature constant in multiple segments [25]. Similarly, optimum fiber angles were converted to manufacturable fiber steering process by the least square and continuity constraint (LSC) method to find the continuous fiber paths [8, 30]. Another approach constrained the norm of the gradient of fiber angle for manufacturing purposes [31]. Likewise, tow-orientated VS plates applied the curvature constraint to design manufacturable curvilinear paths [17]. Apart from those, flow field functions or stream functions were used that imitate fluid flow to achieve continuous manufacturable paths [32, 33].

There has been different approaches to find optimum tow/fiber paths along with man-

ufacturing constraints. The current study focuses on the optimization of the fundamental frequency of composite plates for fiber steering considering manufacturing constraints. The plates included CS and VS designs including two different laminate configurations of balanced and general laminate cases. The maximization of the natural frequency was performed based on lamination parameters as the design variables. These parameters were then converted to tow/fiber angles and stacking sequence by direct search method. Manufacturing constraints were applied using the LSC method to ensure the feasibility of the manufacturing process with a defined curvature constraint. Finally, streamlines were used to generate the tow paths that best match the LSC results to be used as the guide curves for manufacturing the VS composite layup.

Paper is outlined as follows: Section 2 outlines numerical method and optimization approach used to find the optimum fiber directions. Section 3 illustrates the validation process and the results of the optimum frequency obtained before and after LSC approach. In this section, a broad discussion is given on the curvature constraint results, and comparison is presented for CS and VS designs. Section 4 includes the conclusions related with the use of VS designs for different boundary conditions and aspect ratios.

## 2. Numerical Method

The current numerical method consists of FEM method with Bogner, Fox, and Schmit, Rectangular Plate, Element and the optimization process to find the optimum lamination parameters that maximize the fundamental frequency of the composite plate. The resulting lamination parameters either can be different (VS) or the same (CS) within a ply throughout the plate. After this process, the lamination parameters were converted into stacking sequences and fiber angles using direct search method. Then, the fiber angles at each layer was converted into manufacturable fiber angle distributions through the LSC method with a maximum limit on elemental curvatures. Finally these angles were converted into fiber paths, as an input to the AFP machine, using streamline functions. Figure 1 outlines the summary of the numerical method schematically.

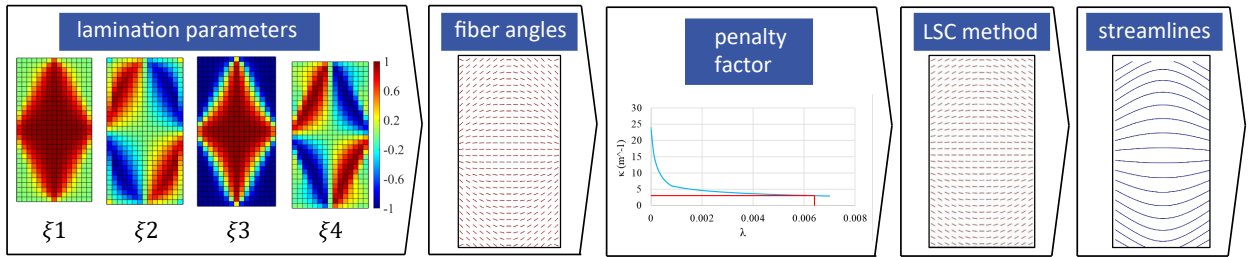


Figure 1: Schematic outline of the numerical method

### 2.1. Finite Element Model

The conforming Bogner-Fox-Schmid type rectangular element type with four degrees of freedom (DOF) per node and a total of sixteen DOF per element is used. The four DOFs are characterized by the out-of-plane displacement, slopes in two in-plane directions and twist

characterize the four DOFs of a node [34]. The interpolation functions are shown in Appendix A.

The fundamental frequency of a plate is computed by solving the generalized eigenvalue problem in Equation (1) in which  $[\mathbf{K}]$ ,  $[\mathbf{M}]$ ,  $\{\mathbf{a}_i\}$ ,  $\lambda_i$  represent the bending stiffness matrix, mass matrix, eigenvectors, and eigenvalues, respectively.

$$([\mathbf{K}] - \lambda_i[\mathbf{M}]) \{\mathbf{a}_i\} = \{\mathbf{0}\} \quad i = 1, 2, \dots, n \quad (1)$$

The frequency of each mode shape,  $f_i$ , is calculated by taking the square root of the eigenvalues, Equation (2).

$$f_i = \sqrt{\lambda_i} \quad (2)$$

Mass matrix is computed using the interpolation functions,  $\{\mathbf{N}\}$ , density of the material,  $\rho$ , and plate thickness,  $t$ , in Equation (3). Mass matrix is constant over the domain ignoring the effect of varying defect content over the plate.

$$[\mathbf{M}] = \int_{\Omega} \{\mathbf{N}\}^T \rho t \{\mathbf{N}\} d\Omega \quad (3)$$

Bending stiffness is assumed for the composite plates, hence stiffness matrix is computed using Equation (4) in which  $[\mathbf{D}]$  is the bending stiffness matrix of the composite laminate.

$$[\mathbf{K}] = \int_{\Omega} [\mathbf{B}]^T [\mathbf{D}] [\mathbf{B}] d\Omega \quad (4)$$

Equation (5) shows the moment-curvature coupling for a composite plate,  $[\mathbf{B}]$ , using the partial derivatives of interpolation function vector,  $\{\mathbf{N}\}$ . In this work, Bogner-Fox-Schmidt type of compatible rectangular finite elements are used.

$$[\mathbf{B}]^T = \begin{bmatrix} \frac{\partial^2 \{\mathbf{N}\}}{\partial x^2} & \frac{\partial^2 \{\mathbf{N}\}}{\partial y^2} & \frac{\partial^2 \{\mathbf{N}\}}{\partial x \partial y} \end{bmatrix} \quad (5)$$

## 2.2. Material Properties

The vectorized form of material stiffness of the laminate,  $\{\mathbf{d}\}$ , is defined in terms of the lamination parameters,  $\{\boldsymbol{\xi}\}$ , as in Equation (6).

$$\{\mathbf{d}\} = \frac{t^3}{12} [\mathbf{U}] \{\boldsymbol{\xi}\} \quad (6)$$

Two different types of stiffness are assumed: **i.** Constant Stiffness (CS); in which the lamination parameters for each element over the domain is the same, and **ii.** Variable Stiffness (VS); in which the lamination parameters of each element can vary. The laminate configurations are categorized into two different types; balanced (orthotropic) or general. Equation (7) shows the lamination parameters for the balanced (orthotropic) case, that is

defined by only two parameters,  $\xi_1$  and  $\xi_3$ .

$$\{\boldsymbol{\xi}\} = \{ \xi_1 \quad 0 \quad \xi_3 \quad 0 \}^T \quad (7)$$

Equation (8) shows the lamination parameters for general VS case that is defined in terms of four different lamination parameters,  $\xi_1$ ,  $\xi_2$ ,  $\xi_3$  and  $\xi_4$ .

$$\{\boldsymbol{\xi}\} = \{ \xi_1 \quad \xi_2 \quad \xi_3 \quad \xi_4 \}^T \quad (8)$$

Equation (9) shows the material invariant matrix,  $[\mathbf{U}]$ , that is independent of the fiber angle or thickness.

$$[\mathbf{U}] = \begin{bmatrix} U_1 & U_2 & 0 & U_3 & 0 \\ U_4 & 0 & 0 & -U_3 & 0 \\ U_1 & -U_2 & 0 & U_3 & 0 \\ 0 & 0 & U_2/2 & 0 & U_3 \\ 0 & 0 & U_2/2 & 0 & -U_3 \\ (U_1 - U_4)/2 & 0 & 0 & -U_3 & 0 \end{bmatrix} \quad (9)$$

The material stiffness matrix invariants are expressed in terms of the lamina stiffness constants of  $Q_{11}$ ,  $Q_{22}$ ,  $Q_{12}$  and  $Q_{66}$  through Equations (10)-(13).

$$U_1 = \frac{3Q_{11} + 3Q_{22} + 2Q_{12} + 4Q_{66}}{8} \quad (10)$$

$$U_2 = \frac{Q_{11} - Q_{22}}{2} \quad (11)$$

$$U_3 = \frac{Q_{11} + Q_{22} - 2Q_{12} - 4Q_{66}}{8} \quad (12)$$

$$U_4 = \frac{Q_{11} + Q_{22} + 6Q_{12} - 4Q_{66}}{8} \quad (13)$$

The lamina stiffness terms are calculated from lamina elastic moduli;  $E_{11}$ ,  $E_{22}$ , Poisson's ratio  $\nu_{12}$ , and shear modulus  $G_{12}$  using Equations (14)-(17).

$$Q_{11} = \frac{E_{11}^2}{E_1 - \nu_{12}^2 E_{22}} \quad (14)$$

$$Q_{12} = \frac{\nu_{12} E_1 E_{22}}{E_1 - \nu_{12}^2 E_{22}} \quad (15)$$

$$Q_{22} = \frac{E_{11} E_{22}}{E_{11} - \nu_{12}^2 E_{22}} \quad (16)$$

$$Q_{66} = G_{12} \quad (17)$$

### 2.3. Optimization

The objective is to maximize the first fundamental frequency,  $\lambda_1$ , Equation (18).

$$\min(-\lambda_1) \quad (18)$$

The optimization design variables are the lamination parameters,  $\{\boldsymbol{\xi}\}$ . The lamination parameters have constraints among them [35, 36]. These constraints are defined as non-linear optimization constraints in the optimization scheme.

*s.t. for balanced (orthotropic) material case:*

$$2\xi_1^2 - \xi_3 \leq 1 \quad (19)$$

$$-1 \leq \xi_3 \leq 1 \quad (20)$$

*s.t. for general material case:*

$$2\xi_1^2(1 - \xi_3) + 2\xi_2^2(1 + \xi_3) + \xi_3^2 + \xi_4^2 - 4\xi_1\xi_2\xi_4 \leq 1 \quad (21)$$

$$\xi_1^2 + \xi_2^2 \leq 1 \quad (22)$$

$$-1 \leq \xi_3 \leq 1 \quad (23)$$

The gradient based optimization uses the sensitivity of the objective function. The sensitivity of  $i$ th eigenvalue,  $\lambda_i$ , with respect to a design variable,  $\{\boldsymbol{\xi}\}$ , is computed by differentiation according to Equation (24). The derivation for this expression can be found in earlier references [37].

$$\frac{\partial \lambda_i}{\partial \{\boldsymbol{\xi}\}} = \{\mathbf{a}_i\}^T \frac{\partial [\mathbf{K}]}{\partial \{\boldsymbol{\xi}\}} \{\mathbf{a}_i\} \quad (24)$$

The differentiation of stiffness matrix in Equation (4) with respect to the design variable (out-of-plane lamination parameters) gives Equation (25).

$$\frac{\partial [\mathbf{K}]}{\partial \{\boldsymbol{\xi}\}} = \int_{\Omega} [\mathbf{B}]^T \frac{\partial [\mathbf{D}]}{\partial \{\boldsymbol{\xi}\}} [\mathbf{B}] d\Omega \quad (25)$$

Equations (26)-(29) show the partial derivative of vectorized bending stiffness,  $[\mathbf{D}]$ , with respect to the components of the lamination parameters,  $\{\boldsymbol{\xi}\}$ .



$$\frac{\partial[\mathbf{D}]}{\partial\xi_1} = \frac{t^3}{12} [\mathbf{U}] \{0 \ 1 \ 0 \ 0 \ 0\}^T \quad (26)$$

$$\frac{\partial[\mathbf{D}]}{\partial\xi_2} = \frac{t^3}{12} [\mathbf{U}] \{0 \ 0 \ 1 \ 0 \ 0\}^T \quad (27)$$

$$\frac{\partial[\mathbf{D}]}{\partial\xi_3} = \frac{t^3}{12} [\mathbf{U}] \{0 \ 0 \ 0 \ 1 \ 0\}^T \quad (28)$$

$$\frac{\partial[\mathbf{D}]}{\partial\xi_4} = \frac{t^3}{12} [\mathbf{U}] \{0 \ 0 \ 0 \ 0 \ 1\}^T \quad (29)$$

After the optimization, the optimum lamination parameters,  $\{\boldsymbol{\xi}_{opt}\}$ , can be converted into fiber angles and stacking sequences by direct search among the possible configurations,  $\{\boldsymbol{\xi}(\theta_{opt}, t)\}$ , Equation (30).

$$\min(|\{\boldsymbol{\xi}(\theta_{opt}, t)\} - \{\boldsymbol{\xi}_{opt}\}|) \quad (30)$$

The optimization and finite element implementations are both prepared in MATLAB<sup>®</sup> environment for efficiency. "fmincon" optimization toolbox with interior-point method is used to ensure the feasibility of the constraints.

#### 2.4. Manufacturing Constraints

The optimum fiber angles are converted into continuous and manufacturable fiber path using LSC method in which fiber angles are treated as the field variable,  $\theta(\mathbf{x})$ , which have the minimum difference from the optimum fiber angles. Therefore, the local form of the least-squares is obtained by Equation (31).

$$\theta(\mathbf{x}) - \theta_{opt} = 0 \quad (31)$$

The continuity is enforced by setting the gradient of the fiber angles to zero. In the extreme situation, when the gradient is zero, composite laminates become CS laminate. This constraint is enforced locally by using Equation (32).

$$\nabla\theta(\mathbf{x}) = \mathbf{0} \quad (32)$$

These two equations can be coupled to solve for the field variable through a penalty factor,  $\alpha$ , that penalizes the continuity constraint, Equation (33).

$$\theta(\mathbf{x}) + \alpha \nabla\theta(\mathbf{x}) \cdot \nabla\theta(\mathbf{x}) = \theta_{opt} \quad (33)$$

Multiplying this equation by weight functions and integrating, we can find the weak form in Equation (34), in which  $\{\boldsymbol{\theta}\}$  is the nodal values of the fiber angles.

$$([\mathbf{L}] + \alpha[\mathbf{C}]) \{\boldsymbol{\theta}\} = \{\mathbf{q}(\theta_{opt})\} \quad (34)$$

Least squares constraint,  $[\mathbf{L}]$ , takes the form in Equation (35) in terms of the weight

functions,  $\{\mathbf{N}_\theta\}$ . The same symbol is used for the interpolation functions and the weight function but the weight function for interpolation of fiber angles need not necessarily be the same function as used for the interpolation of displacements hence they are denoted with the subscript LSC,  $\{\mathbf{N}_\theta\}$ .

$$[\mathbf{L}] = \int_{\Omega} \{\mathbf{N}_\theta\}^T \{\mathbf{N}_\theta\} d\Omega \quad (35)$$

Continuity constraint,  $[\mathbf{C}]$ , becomes as in Equation (36) in terms of the gradient of the weight functions,  $\{\mathbf{N}\}$ .

$$[\mathbf{C}] = \int_{\Omega} \{\nabla \mathbf{N}_\theta\}^T \{\nabla \mathbf{N}_\theta\} d\Omega \quad (36)$$

Optimum fiber angles form a pseudo-force vector that is given by Equation (37).

$$\{\mathbf{q}(\theta_{opt})\} = \int_{\Omega} \{\mathbf{N}_\theta\}^T \theta_{opt} d\Omega \quad (37)$$

The penalty factor for the continuity constraint,  $\alpha$ , is determined for the given limit that is imposed on the maximum of elemental curvatures,  $\kappa_{el}^{max}$ . The elemental curvatures,  $\kappa_{el}$ , is computed using Equation (38). The elemental quantities  $\{\theta_{el}\}$ ,  $[\mathbf{C}_{el}]$ , and  $\omega$  refer to the fiber angle at the nodes, continuity constraint matrix, and the domain (area) of the element under consideration, respectively.

$$\kappa_{el}^2 = \{\theta_{el}\}^T [\mathbf{C}_{el}] \{\theta_{el}\} / 4\omega \quad (38)$$

Further details of this method can be found in the earlier references [8, 30].

## 2.5. Stream functions

The tow paths shall be generated in order to manufacture the composite material using AFP method. The system needs the guide curves as inputs that are continuous polylines. The optimum and LSC method reveal tow angles in discrete form. For this reason, these angles need to be connected through tow paths. This is done by application of stream function method that was developed earlier [38]. The weak form of the same method is obtained in this study to find the flow potentials.

Equation (39) shows the stream function,  $\Psi(x, y)$ , and for each value of  $C$  a streamline can be obtained.

$$\Psi(x, y) = C \quad (39)$$

Blom et al. reduced this problem into a linear form by introducing natural logarithm of thickness function,  $h$ , and given fiber angles,  $\theta$  as in Equation (40).

$$-\mathbf{s} \nabla \ln(h) = \mathbf{n} \nabla \theta \quad (40)$$

In which  $\mathbf{s}$  and  $\mathbf{n}$  represent tangent and normal directions, respectively, in terms of

trigonometric function of the angles.

$$\mathbf{n} = \begin{Bmatrix} -\sin \theta \\ \cos \theta \end{Bmatrix} \quad \nabla \theta = \begin{Bmatrix} \theta_{,x} \\ \theta_{,y} \end{Bmatrix} \quad (41)$$

$$\mathbf{s} = \begin{Bmatrix} \cos \theta \\ \sin \theta \end{Bmatrix} \quad \nabla \ln(h) = \begin{Bmatrix} h_{,x}/h \\ h_{,y}/h \end{Bmatrix} \quad (42)$$

The global form of the linear problem in Equation (42) is obtained by weighting this equality and integrating to give Equation (43). In this relation  $[\mathbf{A}]$ ,  $\{\mathbf{h}\}$ , and  $\{\mathbf{\Theta}\}$  represent the coefficient matrix, logarithm of thickness function, and a vector consisting of given tow angles, respectively.

$$[\mathbf{A}] \{\mathbf{h}\} = \{\mathbf{\Theta}\} \quad (43)$$

### 3. Results and Discussion

The composite laminates with different boundary conditions and aspect ratios were investigated. The optimum fundamental frequency was obtained and the results were converted into composite layups. The optimization was performed in MATLAB<sup>®</sup> with the "fmincon" solver and "interior-point" algorithm to ensure the design variables to remain inside the feasible region. FEA analysis was performed to calculate the higher natural frequencies and mode shapes in order to study the laminate behavior with the optimum fiber angle. A commercial finite element analysis software (ANSYS<sup>®</sup>) was used along with the presented method to validate the in-house developed method for CS cases.

#### 3.1. Optimum frequency analysis

In this study, optimization method is employed to different layup configurations that include; general constant stiffness (general CS), balanced variable stiffness (balanced VS), and general variable stiffness (general VS) layups to provide comparison to the literature findings. The presented methodology was used to simulate the cases presented in the earlier studies related with fundamental frequency optimization to validate the results. The non-dimensional natural frequency was obtained through Equation (44), in which  $b$  represents the shorter edge length of the panel.

$$\bar{f}_1 = f_1 \left( \frac{b^2}{t} \right) \sqrt{\frac{\rho}{E_{22}}} \quad (44)$$

The ratios of material moduli were  $E_{11}/E_{22} = 25$ ,  $G_{12}/E_{22} = 0.5$ , and  $\nu_{12} = 0.25$  as in the reference [14]. Similarly, the material properties for graphite/epoxy lamina were  $E_{11} = 200$  GPa,  $E_{22} = 8$  GPa,  $G_{12} = 4$  GPa, and  $\nu_{12} = 0.25$  as in the reference [39].

Table 1: Comparison of the optimum fundamental frequencies for general CS, balanced VS, and general VS plates for various boundary conditions and aspect ratios with the references [14, 39].

case	aspect ratio	mesh size	BCs	optimum layup	$\bar{f}_1$			imp. [%]	
					ref.	ANSYS <sup>®</sup>	present	ref.	present
gen. CS	1	15x15	SSSS	$[-45^\circ(0.21)/45^\circ(0.79)]_s$	20.57 [39]	20.2	20.6	-	-
bal. VS				-	20.57 [14]	-	20.6	0.0	0.0
general VS				-	22.22 [14]	-	22.5	7.8	9.2
gen. CS	1.5	15x23	SSSS	$[30^\circ(0.21)/-25^\circ(0.79)]_s$	14.83 [39]	14.9	15.1	-	-
bal. VS				-	16.50 [14]	-	16.6	11.5	9.9
gen. VS				-	17.70 [14]	-	18.1	19.6	19.9
gen. CS	2	15x30	SSSS	$[0]_s$	14.46 [39]	14.4	14.5	-	-
bal. VS				-	15.37 [14]	-	15.4	6.2	6.2
gen. VS				-	16.28 [14]	-	16.4	12.4	13.1
gen. CS	2.5	15x37	SSSS	$[0]_s$	14.38 [39]	14.3	14.4	-	-
bal. VS				-	14.89 [14]	-	14.9	3.5	3.5
gen. VS				-	15.60 [14]	-	15.7	8.3	9

Table 1 shows the comparison of the results with the references. The cases include both fully simply-supported (SSSS) and fully clamped (CCCC) boundary conditions as well as different aspect ratios [14, 39]. In this study, the natural frequency for the optimum general CS cases were also repeated by using a commercial finite element software to validate the finding of the in-house model. The optimum fundamental frequency of the general VS composite laminates and balanced VS were significantly higher than that of the optimum fundamental frequency of the general CS cases. For example, the fully simply-supported plate for an aspect ratio of two was designed using the LSC method with the same mesh size as in the reference [14]. The non-dimensional fundamental frequency,  $\bar{f}_1$ , was computed as 14.5, 15.4, and 16.4 for general CS, balanced VS, and general VS cases, respectively, revealing an increase by 6.2% and 13.1% with respect to general CS laminate with  $0^\circ$  layers. The optimum constant stiffness layup had  $0^\circ$  layup, fibers along the shorter width direction, for the maximum frequency. Similarly, significant increase in the natural frequency was obtained by using VS composites over CS layups especially for the fully clamped case, Table 1. fully clamped boundary conditions demand for a more heterogeneous distribution of fibers/tows over the plate that could be possible with VS designs. The improvement of fundamental frequency was much more apparent in general VS design as the fibers can be much more freely distributed in the panel compared to the balanced VS case.

Table 2 shows another comparison of the fundamental frequencies of various laminate designs were calculated for general CS, balanced VS, and general VS designs with the references [5, 14]. The boundary conditions were either fully simply-supported (SSSS) or fully clamped (CCCC). The present model was used to find the optimum fundamental frequencies of the same laminate configurations, Table 2. In addition, a commercial finite element software was used for validation of the CS cases with the in-house code. Non-dimensional frequency,  $\tilde{f}_1$ , was obtain by Equations (45) and (46) in which  $a$  represents the longer side of the panel.

$$\tilde{f}_1 = f_1 a^2 \sqrt{\left(\frac{\rho}{D_0}\right)} \quad (45)$$

$$D_0 = \frac{E_{22} t^3}{12(1 - \nu_{12}\nu_{21})} \quad (46)$$

The material properties were  $E_{11} = 138$  GPa,  $E_{22} = 8.96$  GPa,  $G_{12} = 7.1$  GPa, and  $\nu_{12} = 0.3$  as in the reference [5].

Table 2: Comparison of the optimum fundamental frequencies for CS and general VS plates to the corresponding values in the references [5, 14] for two different boundary conditions and aspect ratios.

case	aspect ratio	mesh size	BCs	optimum layup	$\tilde{f}_1$			imp. [%]	
					ref.	ANSYS®	present	ref.	present
CS	1	8x8	SSSS	[45/-45/-45/-45]s	56.32 [5]	55.7	55.4	8.8%	11.0%
CS				-	55.53 [14]	-	56.6		
VS				-	61.26 [14]	-	61.5		
CS	1	8x8	CCCC	[0/90/90/90]s	93.62 [5]	93.9	93.6	31.2%	30.8%
CS				-	93.62 [14]	-	93.6		
VS				-	122.84 [14]	-	122.4		
CS	2	16x8	SSSS	[90/90/90/90]s	159.89 [5]	159.6	159.9	8.5%	11.5%
CS				-	159.89 [14]	-	159.9		
VS				-	173.52 [14]	-	178.3		
CS	2	16x8	CCCC	[90/90/90/90]s	354.44 [5]	353.2	354.8	2.2%	3.8%
CS				-	354.4 [14]	-	355		
VS				-	362.14 [14]	-	368.3		

VS laminates reveals a significant increase in the natural frequency by steering the fibers in comparison to the CS laminates of the same mass. Present model revealed consistent results for the CS cases with the references [5, 14]. In addition, the comparison of the CS values with the commercially available software demonstrated the reliability of the in-house method. However, the presented method reveals slightly higher optimum frequencies with respect to the corresponding findings in the reference [14] approximately for all of the VS cases. The increase in the fundamental frequency for the fully clamped case with an aspect ratio of unity was the highest, although this effect significantly decreases by changing the aspect ratio.

### 3.2. Optimum lamination parameters

Figure 2 shows the optimum distribution of the lamination parameters for the fully simply-supported VS layup with an aspect ratio of  $L/W=2$ . The optimum normalized fundamental natural frequency was  $\tilde{f}_1=16.4$  for this case. The material properties were the same as in the reference [39].

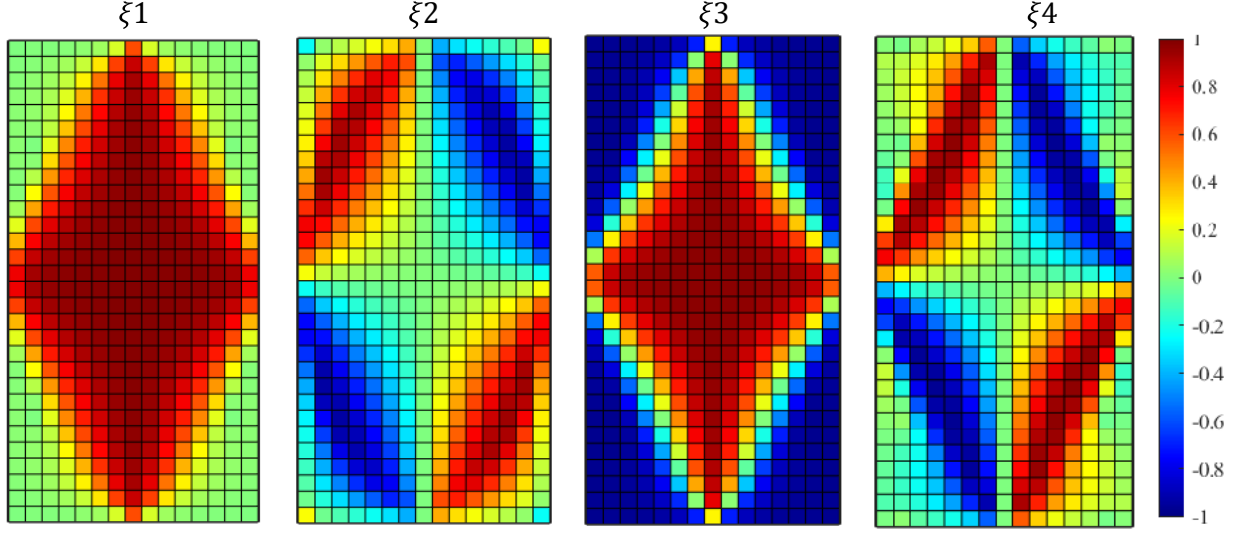


Figure 2: Optimum distribution of the lamination parameters for the fully simply-supported, VS composite with an aspect ratio of  $L/W=2$

The distribution of lamination parameters had a symmetric distribution after optimization. In the plots the distribution appears as two-fold symmetric. However, the sign of the lamination parameters alternating due to the change changing sign of the fiber angles when a single layer situation considered for simplicity. Therefore, the results were four-fold symmetric indeed those were consistent with the natural symmetry of the plate.

The optimization was also performed by using random initial guesses for the lamination parameters in the elements. In general zero initial values were used as the initial values of the lamination parameters to start from the center of the feasible region for the lamination parameter space. However, the method reveals exactly the same results independent of the initial guesses that shows the robustness of the presented method.

Figure 3 shows the optimum distribution of lamination parameters for the fully clamped boundary condition of the general VS case. Similarly, the optimum result had a four-fold symmetric distribution.

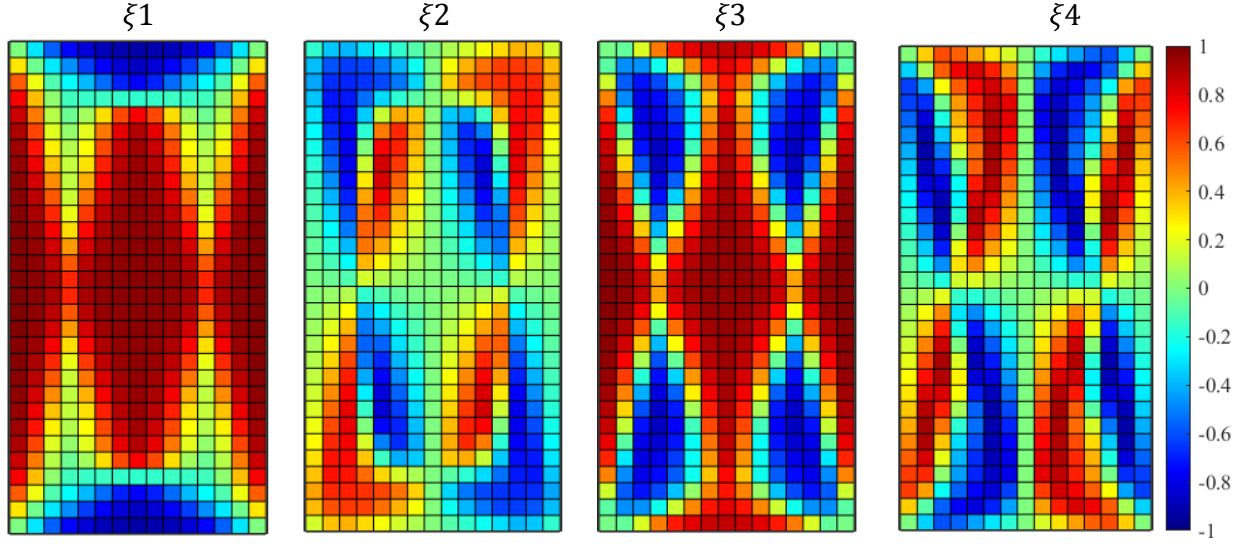


Figure 3: Optimum distribution of the lamination parameters for the fully clamped, VS composite with an aspect ratio of  $L/W=2$

### 3.3. Mesh sensitivity

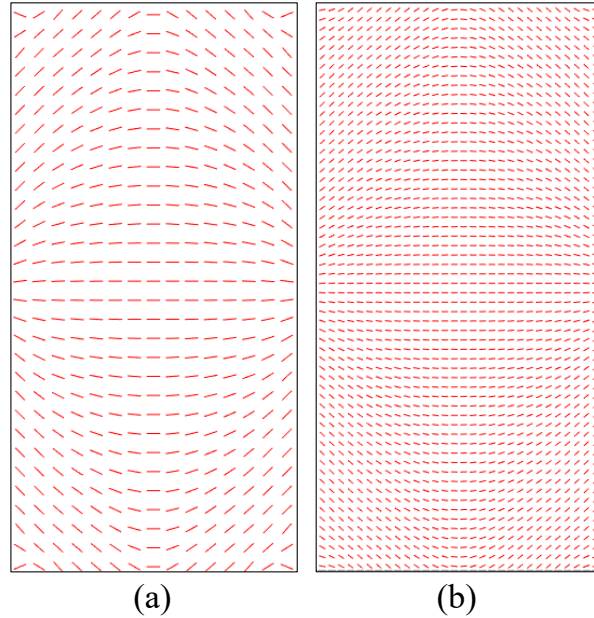


Figure 4: Optimum fiber distribution for the fully simply-supported, VS laminate with an aspect ratio of  $L/W=2$  for the (a) original mesh size of  $15 \times 30$  and (b) refined mesh size of  $30 \times 60$ .

The mesh sensitivity of the fully simply-supported, general VS case with an aspect ratio of  $L/W=2$  was analyzed by subdividing the mesh by two along both longitudinal and transverse directions. Figure 4 shows the fiber angles and their distribution for the coarse

and fine meshes. The angles were obtained by direct search method from the optimum lamination parameters as explained earlier. The overall curvature and their distributions were approximately the same for the original and the refined mesh. However, the magnitudes of elemental curvatures were different because of the changing element size. The mesh refinement did not alter the fiber angle distributions hence, the different cases were studied with the coarse mesh size as in the reference [14]. This mesh independent behavior of the optimization reveals the reliability and strength of the proposed approach.

### 3.4. Optimum mode shapes

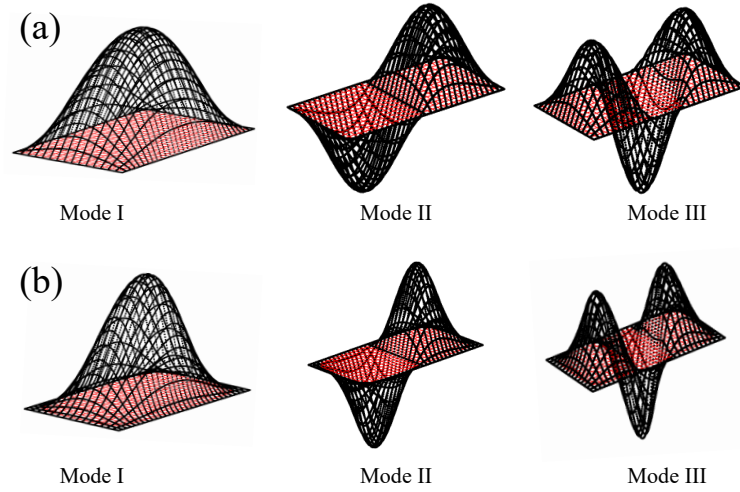


Figure 5: The first three mode shapes of the (a) fully simply-supported and (b) fully clamped VS composite panels with aspect ratio of  $L/W=2$

Figure 5 shows the first three mode shapes of the variable stiffness (VS) panel with fully simply-supported and fully clamped boundary conditions and aspect ratio of  $L/W = 2$ . These mode shapes were obtained from the optimum layup sequence for fundamental frequency of the composite panel. Since the first natural frequency is of the highest relevance in dynamics point of view, the composite layup was optimized for the fundamental frequency. The second and third modes were calculated and analyzed for the same layup. The prediction of higher natural frequencies would be beneficial to study the composite panel behavior. Another concern related to mode shape analysis is the coincidence of the frequencies in higher modes. This would lead to undesirable consequences related with resonance that could destroys the structure, hence it is unwanted.

### 3.5. Least-Squares and Continuity Constraints (LSC method)

LSC method was used to maintain the continuity of the fiber/tow angle distributions. In addition, the LSC method was employed to limit the curvatures with a penalty factor approach. Tow steering process to manufacture VS composites has curvature limits that needs to be considered in the design stage. Therefore, the LSC method finds fiber angle distributions that best match the optimum results while satisfying the curvature limits.



Therefore, the resulting fiber angle distributions will be different than the optimum angles revealing a lower performance than the optimum.

The method results are described in the following order. First the method to find the penalty parameter is explained. Next, fiber angle distributions and the effect of penalty parameters are shown. Then, the elemental curvature distributions are shown to illustrate the application of curvature limit. Finally the resulting changes in the objective function is compared with the optimum findings to determine the effectiveness of the proposed approach.

### 3.5.1. Penalty parameter determination

The penalty factor was applied to enforce a limit on the maximum value of the curvatures. In the diagram of Figure 6(a), the penalty parameter  $\lambda = 0$  depicts the fiber angle distribution without the curvature limit. This may cause discontinuities and sharp changes in between the tows that are next to each other. In this figure, the curvature limit starts from its maximum  $\kappa = 24 \text{ m}^{-1}$  and descends with an increase in the penalty parameter  $\lambda$ .

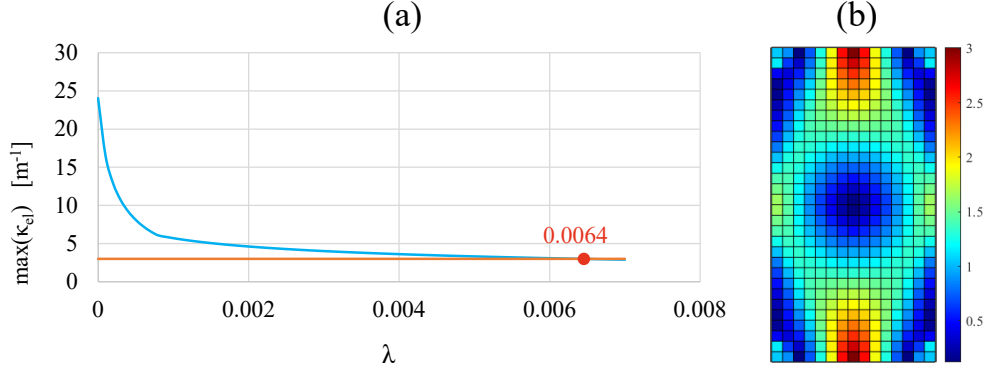


Figure 6: Penalty parameter calculation based on curvature limit of  $3 \text{ m}^{-1}$  for fully simply-supported VS composite panel with aspect ratio of  $L/W = 2$  and optimized frequency of  $\bar{f}_1 = 16.4$

As the penalty parameter increases, the curvature constraint enforces the fiber angles to align parallel with each other in the extreme leading to a constant stiffness plate. Therefore, the penalty parameter needs to be identified. For the fully simply-supported VS composite with an aspect ratio of  $L/W = 2$ , in Figure 6(b) shows that the penalty parameter  $\lambda = 0.0064$  satisfies  $\kappa = 3 \text{ m}^{-1}$ . In current study, the same analysis was applied to all of the layups and this way a different value of penalty parameter was obtained for each case.

### 3.5.2. Fiber angle distribution - LSC method

Figure 7 shows the fiber angle distribution for a fully simply-supported VS composite panel with an aspect ratio of  $L/W = 2$ . The fiber angles before the application of the LSC method is shown for  $\lambda = 0$  case. Increasing the penalty parameter gradually reduces the curvature and finally revealing a constant stiffness design. The optimum penalty parameter for the given constraint,  $\lambda = 0.0064$ , was applied to the analysis, and the corresponding fiber angle distribution was computed.

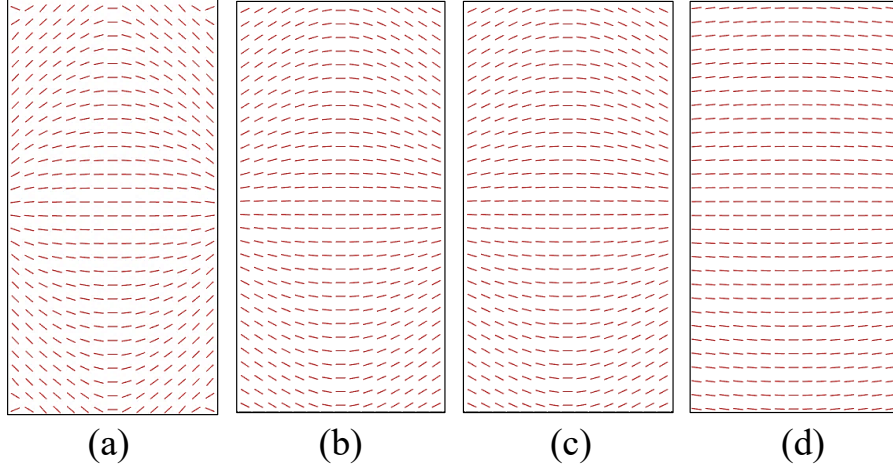


Figure 7: Optimum fiber angle distribution for fully simply-supported VS composite panel with an aspect ratio of  $L/W = 2$  for various penalty parameters (a) before LSC, (b)  $\lambda=0.0064$ , (c)  $\lambda=0.01$ , (d)  $\lambda=0.1$ .

The LSC method reveals similar results as the optimum solution. Figure 7 without curvature constraint gives a fiber angle distribution that is very close to the optimum distribution for the same case as in Figure 4(a). The least-squares mapping gives the best fit to the optimum result. However, the curvature constraint when applied reveals a different result than the optimum. Therefore, the LSC method always compromise from the objective function.

### 3.5.3. Elemental curvature - LSC method

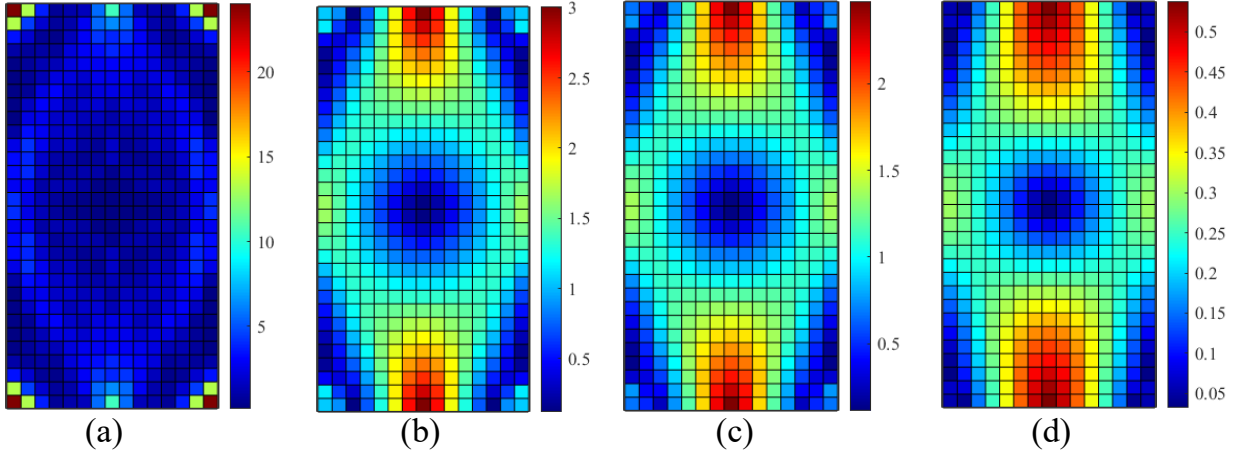


Figure 8: Optimum elemental curvature distribution for fully simply-supported VS composite panel with aspect ratio of  $L/W = 2$  (a) before LSC, (b)  $\lambda=0.0064$ , (c)  $\lambda=0.01$ , (d)  $\lambda=0.1$ .

Figure 8 shows the elemental curvature distribution for different different magnitudes of penalty factors. The maximum curvature with the red color depicts the critical values of curvatures. Elemental curvatures were enforced in the method rather than the overall average curvature since these local regions with high curvature were critical from manufacturing point

of view. The center of the panel with blue color shows the fibers with radius of far more than the critical radius that is consistent with the straight fibers at those locations as shown in Figure 7. The top and bottom areas of the plate contain regions with high magnitudes of curvature that were close to the limit. The curvatures were consistent with the findings in Figure 7.

#### 3.5.4. Optimum frequency analysis - LSC method

Table 3 shows the first three natural frequencies of optimized balanced VS and general VS composite panels that also provides comparison to the reference [14] together with the results of the present method after the application of curvature constraint. The increase in the fundamental frequencies after LSC method with respect to the optimum constant stiffness design were computed. Best improvement in the fundamental frequency was obtained for the SSSS plate with the aspect ratio of  $L/W = 1.5$ . The use of general VS material revealed significant improvement in relation to the balanced VS case as expected. It was efficient to use the VS panels for most cases, but there were cases with little or no improvement in fundamental frequency due to the manufacturing constraints, for which it is better to apply CS designs because it is much more convenient and cost-effective.

Table 3: First three natural frequencies of the optimized case for different aspect ratios of fully simply-supported plates and its comparison to the reference [14]. The LSC method was used with a curvature limit of  $3 \text{ m}^{-1}$ . Improvement with respect to the optimized CS result is indicated in percentage.

type	aspect ratio	BCs	optimum $\bar{f}_{1,2,3}$						$\lambda$	$f_1$ after LSC	imp. [%]
			$\bar{f}_1$ [14]	$\bar{f}_2$ [14]	$\bar{f}_3$ [14]	$\bar{f}_1$	$\bar{f}_2$	$\bar{f}_3$			
CS	1	SSSS	20.57	46.71	46.71	20.6	47.1	47.1	-	-	-
Balanced VS			20.57	47.06	47.06	20.6	47.1	47.1	0.0006	20.6	0.0
General VS			22.22	44.50	44.50	22.5	41.5	41.5	0.0126	19.3	-6.3
CS	1.5	SSSS	14.83	26.63	42.22	15.1	24	36	-	-	-
Balanced VS			16.50	22.25	32.11	16.6	22.1	32.2	0.0023	16.5	9.3
General VS			17.70	22.70	32.10	18.1	21.7	31.1	0.0056	16.9	11.9
CS	2	SSSS	14.46	15.23	17.04	14.5	15.2	17.1	-	-	-
Balanced VS			15.37	17.86	23.28	15.4	18	23.5	0.0025	14.5	0
General VS			16.28	17.99	22.92	16.4	18	22.8	0.0064	15.9	9.7
CS	2.5	SSSS	14.38	14.82	15.80	14.4	14.8	15.8	-	-	-
Balanced VS			14.89	16.20	19.40	14.9	16.3	19.7	0.0024	14.4	0
General VS			15.60	16.31	18.84	15.7	16.5	19.2	0.0069	15.3	6.3

Higher order fundamental frequencies were also investigated for fully simply-supported plate, Table 3. The second and the third frequencies of the plates the aspect ratio of  $L/W = 1$  were coincident. This is expected due to the symmetry of a square panel. The optimization method not only increases the higher frequencies but also pushes the second and third frequencies further away from each other for the cases with higher aspect ratios that are greater than  $L/W = 1.5$ .

Table 4: First three natural frequencies of the optimized case for different aspect ratios of fully clamped plates and its comparison to the reference [14]. The LSC method was used with a curvature limit of  $3 \text{ m}^{-1}$ . Improvement with respect to the optimized CS result is indicated in percentage.

type	aspect ratio	BCs	optimum $\bar{f}_{1,2,3}$						$\lambda$	$f_1$ after LSC	imp. [%]
			$\bar{f}_1$ [14]	$\bar{f}_2$ [14]	$\bar{f}_3$ [14]	$\bar{f}_1$	$\bar{f}_2$	$\bar{f}_3$			
CS	1	CCCC	33.43	69.18	69.18	33.4	48.6	79.2	-	-	-
Balanced VS			41.93	75.01	75.01	42.7	73	73	0.0167	36.8	10.2
General VS			44.26	73.54	73.54	45.8	70.1	70.1	0.0225	35.6	6.6
CS	1.5	CCCC	32.64	33.96	37.20	32.7	34.1	37.4	-	-	-
Balanced VS			34.21	39.36	50.55	34.6	40.3	53	0.0136	32.6	-0.3
General VS			35.48	40.70	53.00	36.2	40.6	54.1	0.0143	33.2	1.5
CS	2	CCCC	32.47	33.02	34.30	32.5	33.1	34.4	-	-	-
Balanced VS			32.98	34.64	38.56	32.2	33.3	40.3	0.0080	31.7	-2.5
General VS			33.84	35.10	38.99	34	35.5	40.4	0.0179	32.7	0.6
CS	2.5	CCCC	32.41	32.70	33.34	32.4	32.7	33.4	-	-	-
Balanced VS			32.62	33.35	35.00	32.8	33.7	36.1	0.0075	31.3	-3.4
General VS			33.16	33.69	35.28	33	33.9	36.1	0.0155	32.5	0.3

Table 4 shows the fully clamped plates with different aspect ratios by giving comparison to the reference [14]. The optimum values of fundamental frequencies were in well agreement with the reference. The application of LSC method reduced the improvement in the fundamental frequencies. For fully clamped case with the aspect ratio of  $L/W = 1$ , the optimum fundamental frequency after the application the curvature limit revealed frequencies that were 6.6% higher than the panel with constant stiffness design of the same boundary conditions. Contrary to the fully simply-supported case, as the aspect ratio increases, the LSC method reduces the frequency gains obtained by the use of VS design. Therefore, the use of VS provides benefits for the low aspect ratio but, CS designs shall be preferred for the fully clamped plates with higher aspect ratios.

Table 5: Natural frequencies of the optimized laminates and frequency improvement after applying LSC method with curvature limit of  $3 \text{ m}^{-1}$  for general VS composite panels and their comparison to the reference [14]. Improvement with respect to the optimized CS result is indicated in percentage.

Ref.	aspect ratio	BCs	initial $\tilde{f}_1$				$\lambda$	$f_1$ after LSC	imp. [%]
			$\tilde{f}_1$ [14]	$\tilde{f}_1$	$\tilde{f}_2$	$\tilde{f}_3$			
General VS	1	SSSS	61.26	61.5	118	118.2	0.0062	53.9	-4.8
General VS	1	CCCC	122.84	122.4	196.2	196.2	0.0179	99.6	6.4
General VS	2	SSSS	173.52	178.3	201.2	262.7	0.0082	169.8	6.2
General VS	2	CCCC	362.14	368.3	390	446.7	0.0128	356.2	0.3

Table 5 shows an additional comparison to the references [5, 14]. Normalization of frequencies was performed using Equation (44) for this comparison. This is a detailed version of the comparison that was presented in Table 2. The optimization results were consistent with the literature findings. The application of manufacturability constraints reduced the improvement in the frequencies below 10%. The decision of using VS design over CS design shall be evaluated carefully by investigated of the case considering manufacturing limitations.

### 3.5.5. Effect of aspect ratio on fiber angle distribution after LSC

The effect of aspect ratio on the resulting fiber angle distributions is further discussed in detail in the context of manufacturability. Figure 9 shows fully simply-supported panels with

aspect ratios of  $L/W = 1.5, 2, 2.5$  and the corresponding optimum fiber angle distributions. The fiber distributions in all panels were designed for maximizing the first natural frequency. The elemental curvature plots of the panels shows the elemental distribution of curvatures from the fiber angles.

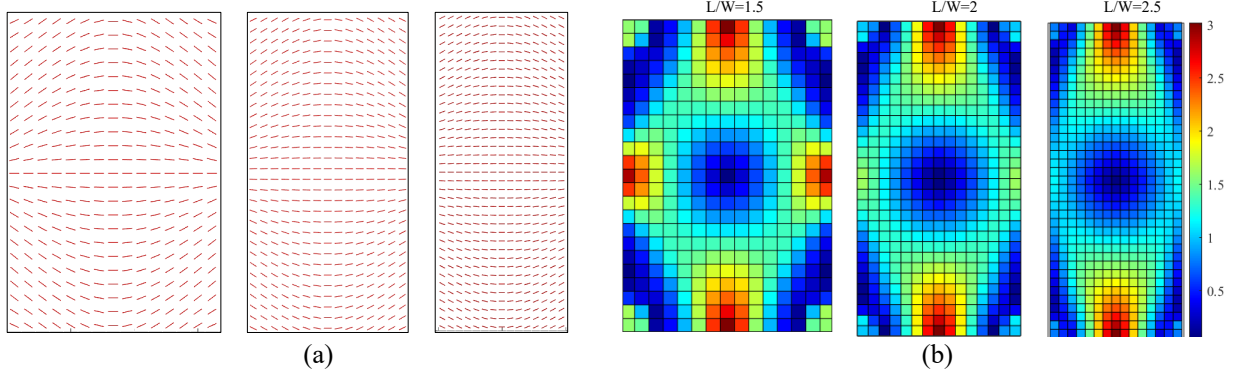


Figure 9: Optimum (a) fiber angle and (b) elemental curvature distribution for fully simply-supported VS panels with aspect ratios of 1.5, 2, and 2.5 with a curvature limit of  $3 \text{ m}^{-1}$ .

The present method employed the maximum curvature limit to panels to find the fiber angle distributions. The panel with aspect ratio of  $L/W = 1.5$  includes greater amount of critical regions at the top, bottom, left, and right sides of the panel, Figure 9. As the aspect ratio increases, the critical area diminishes increasing the areas are occupied by fiber paths with larger radius or smaller curvature. The fundamental frequency reduces after the application of the LSC method of 4.4%, 3%, and 2.5% for the panels with aspect ratios of  $L/W = 1.5, 2, 2.5$ , respectively. It can be concluded that the panels containing greater amount of critical regions with the maximum curvature experienced more significant drops in the fundamental frequency after the application of the LSC method. The panels with higher aspect ratio have little frequency variation after the application of curvature constraint, thereby making the LSC method more effective.

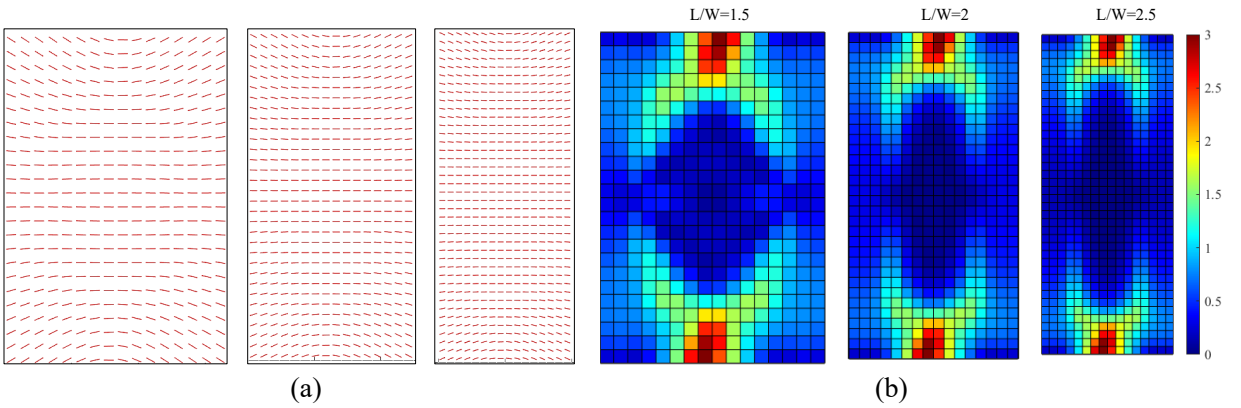


Figure 10: Optimum (a) fiber angle and (b) elemental curvature distribution for fully clamped, VS composite panel for aspect ratios ( $L/W$ ) of 1.5, 2, and 2.5 after the application of the LSC method with the curvature limit of  $3 \text{ m}^{-1}$ .

Figure 10 shows the fiber angle distributions and elemental curvatures for panels with fully clamped boundary conditions. The same observation as in the fully simply-supported case also exists for this case. As the aspect ratio increases, the critical areas with minimum radius decreases. The critical region in the panel with  $L/W=2.5$  covers far less area than the panel with  $L/W=1.5$ . The frequency reductions of 8.3%, 3.8%, and 1.5% were observed for the panels with aspect ratios of  $L/W=1.5$ , 2, and 2.5, respectively. It can be concluded that the a relatively small decrease in the fundamental frequency can be attained by using VS design for higher aspect ratios.

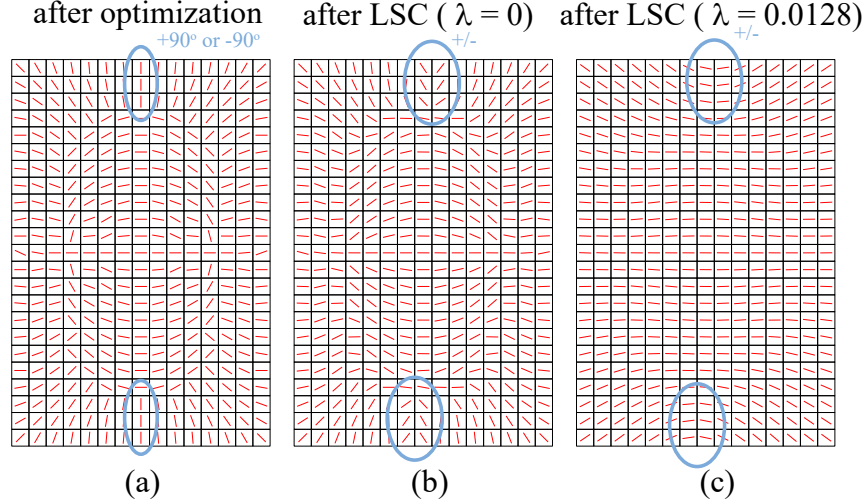


Figure 11: Optimum elemental fiber/tow angle distribution for fully clamped VS composite panel with aspect ratio of  $L/W = 1.5$  (a) before LSC, (b)  $\lambda=0$ , and (c)  $\lambda=0.0128$ .

The angle and curvature distributions in Figure 10 for CCCC case posses a two-fold symmetry rather than the central symmetry observed for the SSSS case in Figure 9. This is not related either with the number of elements or the optimization convergence. Figure 11(a)-11(b)-11(c) show fiber angle distributions for optimum, after the application of LSC method without continuity ( $\alpha = 0$ ) and with the continuity constraint ( $\alpha=0.0128$ ) for the fully clamped plate. The optimum distribution for CCCC case have indeed a quite symmetric result, Figure 11(a). However, application of the LSC method converted the symmetric results with an offset at the marked locations, Figure 2(b). This is definitely not due the continuity constraint since  $\lambda$  has no effect, Figure 2(c). The reason for this is linked with the selected range of the tow/fiber angles that is;  $-90^\circ \leq \theta < 90^\circ$ . Physically there is not a difference between a  $-90^\circ$  and a  $90^\circ$  lamina, but during LSC which involves interpolation and summation of these scalar values, the difference causes the offset from the central-symmetry. Therefore, the inevitable discontinuity in the range of fiber/tow angles causes the disturbance in the symmetry of the results.

### 3.6. Stream function fits prior to manufacturing

The paths for tows are needed for manufacturing the composite material. The AFP machine uses polylines as the input guide curves. Therefore, stream functions used the

outputs of the LSC method to compute the tow directions. Figure 12 shows the results for different fiber angle distributions that were obtained by the optimization for fully simply-supported case. The pure optimization results contain curvatures near the corners of the plate that would be impossible to manufacture, 12(a). However, the LSC method through application of the manufacturing constraint converts the tow paths into manufacturable form by more penalization of large curvatures by using greater values for penalty factor,  $\lambda$ . As the penalty factor increases, the tow paths become smoother with having less curvature. Eventually the tow paths converge to a straight line in the extreme case of full enforcement of curvature constraint as shown in Figure 12 (d). The optimum fiber paths were for the curvature constraint of  $3 \text{ m}^{-1}$  was obtained by using  $\lambda = 0.0064$ , Figure 12(b).

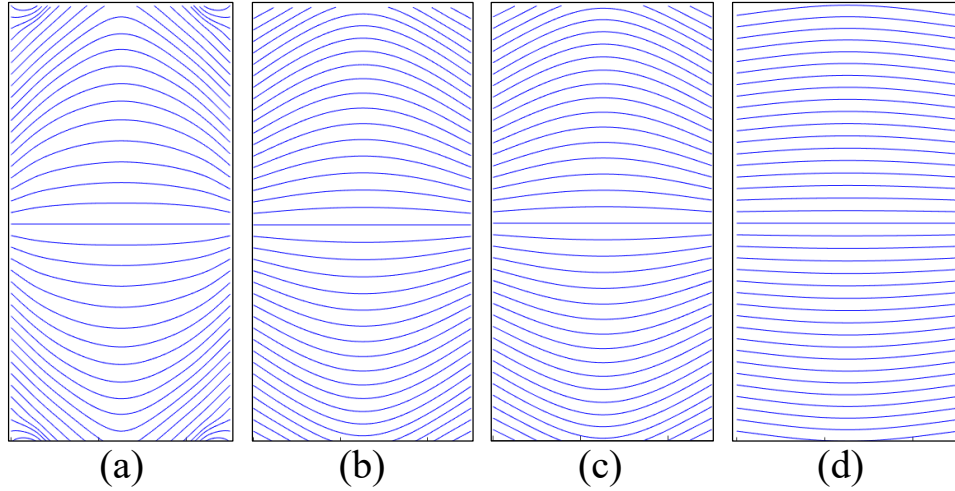


Figure 12: Optimum fiber paths for fully simply-supported VS composite panel with aspect ratio of  $L/W = 2$  for penalty parameters (a) before LSC, (b)  $\lambda=0.0064$ , (c)  $\lambda=0.01$ , (d)  $\lambda=0.1$ .

Stream functions help to convert the discrete tow/fiber angles into continuous paths. The streamlines will then be used for the guide curves that are necessary for manufacturing variable stiffness composites with AFP process.

In the present approach we did not consider the thickness variation due to tow steering. As we push the design toward a constant stiffness plate, this variation will eventually disappear. But during steering thickness variation as well as gaps and overlaps start to occur. These defects are believed to be secondary. On the other hand, lamination parameters are not just a function of the tow angles but also the overall laminate thickness. In some studies thickness is optimized with or without the tow/fiber angles. Besides, for the thickness optimization as the design case, the manufacturing constraints are quite different that focus on ply-drop offs as well as the objective function which is the failure performance. In the current work, the changes in the thicknesses, gaps and overlaps that occur due to tow steering are ignored. Because these defects have secondary influence which were experimentally investigated recently in the reference [40].

## 4. Conclusions

A methodology is presented to design manufacturable composites by tow steering process. The method is applied to design CS, balanced VS, and general VS laminates with fully simply-supported and fully clamped boundary conditions for different aspect ratios. The method reveals the following important conclusions:

- The optimization that uses lamination parameters reveals results that are in agreement with the literature findings. The slight deviations from the literature findings were due to difference in the discretization of optimization variables.
- The curvature constraint in LSC method reveals a manufacturable continuous fiber/tow angle distribution that is different than the optimum distribution thereby leading to a decrease in the fundamental frequency.
- LSC method when applied on fiber/tow angles that have discontinuities due the limited range causes disruption in the symmetry of the results, hence LSC method can better be applied directly to the lamination parameters instead of fiber/tow angles.
- The improvements of 11.9% and 10.2% in the fundamental frequencies of fully simply-supported and fully clamped plates were determined by using LSC method with respect to their optimum constant stiffness cases, respectively.
- The decision to use VS design over CS designs shall be performed carefully by considering manufacturability. The aspect ratio of the plates had significant influence on the optimum results when manufacturability is imposed by the presented LSC method that hamper the benefits of using a VS design.
- The stream function analysis successfully converts the discrete fiber angles into paths that is the basic input for the AFP machines.

The future extension of this method will be buckling and it real applications that includes the manufacturing and testing steered plates.

## 5. Acknowledgment

The authors are grateful for the funding received from The Scientific and Technological Research Council of Turkey (TUBITAK) under Primary Subjects R&D Funding Program (1003) with grant number 218M715.

## A. Interpolation functions

The interpolation function vector is constructed using the shape function components, Eq. (47).

$$\mathbf{N} = \{ N_1 \quad \cdots \quad N_{16} \}^T \quad (47)$$



The sixteen interpolation functions for Bogner-Fox-Schmid elements are shown in the below Eqs. (48)-(63).  $s, t; a, b$  are the parametric coordinates; and the dimensions of the element along  $x$  and  $y$  directions, respectively. Details can be found in the reference [34].

$$N_1 = \frac{1}{16} (s-1)^2 (s+2) (t-1)^2 (t+2) \quad (48)$$

$$N_2 = \frac{1}{16} b (s-1)^2 (s+2) (t-1)^2 (t+1) \quad (49)$$

$$N_3 = \frac{1}{16} a (s-1)^2 (s+1) (t-1)^2 (t+2) \quad (50)$$

$$N_4 = \frac{1}{16} ab (s-1)^2 (s+1) (t-1)^2 (t+1) \quad (51)$$

$$N_5 = -\frac{1}{16} (s-2) (s+1)^2 (t-1)^2 (t+2) \quad (52)$$

$$N_6 = -\frac{1}{16} b (s-2) (s+1)^2 (t-1)^2 (t+1) \quad (53)$$

$$N_7 = \frac{1}{16} a (s-1) (s+1)^2 (t-1)^2 (t+2) \quad (54)$$

$$N_8 = \frac{1}{16} ab (s-1) (s+1)^2 (t-1)^2 (t+1) \quad (55)$$

$$N_9 = \frac{1}{16} (s-2) (s+1)^2 (t-2) (t+1)^2 \quad (56)$$

$$N_{10} = -\frac{1}{16} b (s-2) (s+1)^2 (t-1) (t+1)^2 \quad (57)$$

$$N_{11} = -\frac{1}{16} a (s-1) (s+1)^2 (t-2) (t+1)^2 \quad (58)$$

$$N_{12} = \frac{1}{16} ab (s-1) (s+1)^2 (t-1) (t+1)^2 \quad (59)$$

$$N_{13} = -\frac{1}{16} (s-1)^2 (s+2) (t-2) (t+1)^2 \quad (60)$$

$$N_{14} = \frac{1}{16} b (s-1)^2 (s+2) (t-1) (t+1)^2 \quad (61)$$

$$N_{15} = -\frac{1}{16}a(s-1)^2(s+1)(t-2)(t+1)^2 \quad (62)$$

$$N_{16} = \frac{1}{16}ab(s-1)^2(s+1)(t-1)(t+1)^2 \quad (63)$$

## B. Benchmark for the in-house code

In this section, modal analysis of the optimum constant stiffness panel is shown. The optimum layup was obtained for the constant stiffness panel for fully simply-supported and fully clamped boundary conditions and aspect ratio of  $L/W = 2$  in ANSYS<sup>®</sup> software. The layup was used to validate the frequency results, Figure 13.

- *Element type*: The element type used in this study was "SHELL281" that was suitable for analyzing thin to moderately-thick shell structures. This element consists of eight nodes, and each node has six degrees of freedom for translations and rotations about x, y, and z axes. This type of element is used for modeling composite shells with multiple layers [41]. The element stiffness was set to bending and membrane.
- *Material properties*: The material properties were as follows:  $E_{11} = 200$  GPa,  $E_{22} = 8$  GPa,  $G_{12} = 4$  GPa,  $\nu_{12} = 0.25$ ,  $\rho = 1910$  kg/m<sup>3</sup>.
- *Laminate layup*: The laminate was made up of single layer with  $t = 5$  mm total thickness. The length of the laminate is  $L = 1$  m and the width is  $W = 0.5$  m. This laminate has zero degree of fibers, i.e. the fibers are parallel in transverse direction. The layer properties are given in Figure 13(c).
- *Mesh*: The composite laminate was meshed with the number of 15x30 elements in transverse and longitudinal directions, respectively, Figure 13(b).
- *Boundary conditions*: The laminate considered in this section includes symmetric laminate with fully simply-supported boundary conditions. In order to apply the simply-supported boundary condition, the translation in three global coordinate axes were restrained, Figure 13(b).
- *Analysis type*: The analysis chosen for extracting the natural frequencies of the laminate was the modal analysis. The algorithm used for the analysis was the block Lanczos eigensolver. This algorithm is an eigensolver to determine the structure's natural frequencies and mode shapes.
- *Frequency results*: The first three natural frequencies for fully simply-supported case were  $\omega_1 = 93.9$  Hz,  $\omega_2 = 98.9$  Hz,  $\omega_3 = 110.6$  Hz, respectively. The non-dimensional frequencies were  $f_1 = 14.4$ ,  $f_2 = 15.2$ ,  $f_3 = 17$ , respectively, that are exactly the same in the in-house MATLAB<sup>®</sup> solver.
- *Mode shapes*: The corresponding mode shape of the third natural frequency for fully simply-supported boundary condition is plotted in Figure 13(a).

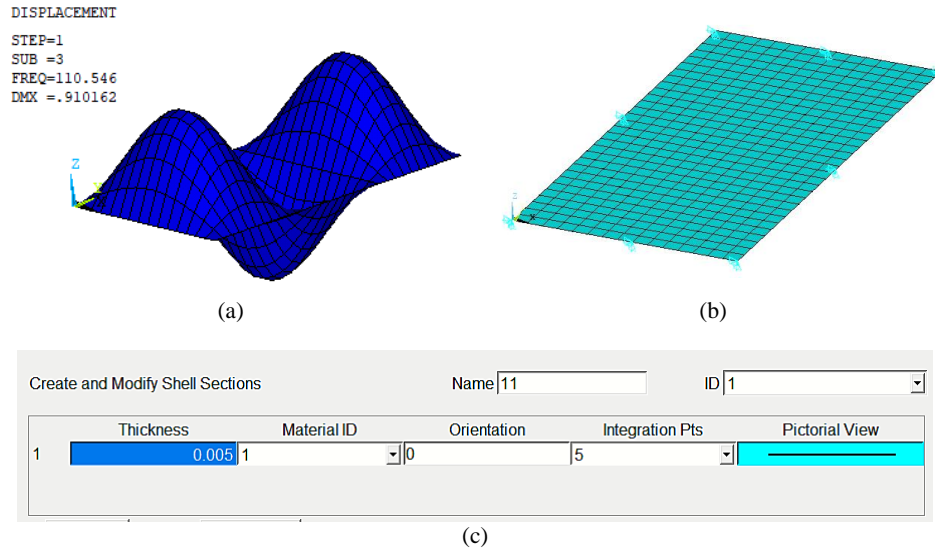


Figure 13: a) third mode shape b) laminate mesh and boundary condition c) layup of single-layer panel with fully simply-supported boundary condition.

## References

- [1] M. H. Nguyen, A. A. Vijayachandran, P. Davidson, D. Call, D. Lee, A. M. Waas, Effect of automated fiber placement (afp) manufacturing signature on mechanical performance of composite structures, *Composite Structures* 228 (2019) 111335.
- [2] E. Oromiehie, B. G. Prusty, P. Compston, G. Rajan, Automated fibre placement based composite structures: Review on the defects, impacts and inspections techniques, *Composite Structures* 224 (2019) 110987.
- [3] E. Lemaire, S. Zein, M. Bruyneel, Optimization of composite structures with curved fiber trajectories, *Composite Structures* 131 (2015) 895–904.
- [4] M. A. Albazzan, R. Harik, B. F. Tatting, Z. Gürdal, Efficient design optimization of nonconventional laminated composites using lamination parameters: A state of the art, *Composite Structures* 209 (2019) 362–374.
- [5] Y. Narita, Layerwise optimization for the maximum fundamental frequency of laminated composite plates, *Journal of Sound and Vibration* 263 (5) (2003) 1005 – 1016, arthur W. Leissa 70th Birthday Issue. doi:[https://doi.org/10.1016/S0022-460X\(03\)00270-0](https://doi.org/10.1016/S0022-460X(03)00270-0).
- [6] K. Sivakumar, N. Iyengar, K. Deb, Optimum design of laminated composite plates with cutouts using a genetic algorithm, *Composite Structures* 42 (3) (1998) 265 – 279. doi:[https://doi.org/10.1016/S0263-8223\(98\)00072-5](https://doi.org/10.1016/S0263-8223(98)00072-5).
- [7] S. Setoodeh, M. M. Abdalla, Z. Gürdal, Design of variable-stiffness laminates using lamination parameters, *Composites Part B: Engineering* 37 (4) (2006) 301 – 309. doi:<https://doi.org/10.1016/j.compositesb.2005.12.001>.

- [8] E. Demir, P. Yousefi-Louyeh, M. Yildiz, Design of variable stiffness composite structures using lamination parameters with fiber steering constraint, *Composites Part B: Engineering* 165 (2019) 733 – 746. doi:<https://doi.org/10.1016/j.compositesb.2019.02.004>.
- [9] J. Sliseris, K. Rocens, Optimal design of composite plates with discrete variable stiffness, *Composite Structures* 98 (2013) 15 – 23. doi:<https://doi.org/10.1016/j.compstruct.2012.11.015>.
- [10] S. Setoodeh, M. M. Abdalla, S. T. IJsselmuiden, Z. Gürdal, Design of variable-stiffness composite panels for maximum buckling load, *Composite structures* 87 (1) (2009) 109–117.
- [11] Z. Wu, P. M. Weaver, G. Raju, B. C. Kim, Buckling analysis and optimisation of variable angle tow composite plates, *Thin-walled structures* 60 (2012) 163–172.
- [12] M. Arian Nik, K. Fayazbakhsh, D. Pasini, L. Lessard, Surrogate-based multi-objective optimization of a composite laminate with curvilinear fibers, *Composite Structures* 94 (8) (2012) 2306 – 2313. doi:<https://doi.org/10.1016/j.compstruct.2012.03.021>.
- [13] S. Honda, T. Igarashi, Y. Narita, Multi-objective optimization of curvilinear fiber shapes for laminated composite plates by using nsga-ii, *Composites Part B: Engineering* 45 (1) (2013) 1071–1078.
- [14] M. M. Abdalla, S. Setoodeh, Z. Gürdal, Design of variable stiffness composite panels for maximum fundamental frequency using lamination parameters, *Composite Structures* 81 (2) (2007) 283 – 291. doi:<https://doi.org/10.1016/j.compstruct.2006.08.018>.
- [15] G. Serhat, B. Bediz, I. Basdogan, Unifying lamination parameters with spectral-tchebychev method for variable-stiffness composite plate design, *Composite Structures* 242 (2020) 112183. doi:<https://doi.org/10.1016/j.compstruct.2020.112183>.
- [16] D. Pereira, T. Sales, D. Rade, Multi-objective frequency and damping optimization of tow-steered composite laminates, *Composite Structures* 256 (2021) 112932. doi:<https://doi.org/10.1016/j.compstruct.2020.112932>.
- [17] H. Akhavan, P. Ribeiro, Natural modes of vibration of variable stiffness composite laminates with curvilinear fibers, *Composite Structures* 93 (11) (2011) 3040 – 3047. doi:<https://doi.org/10.1016/j.compstruct.2011.04.027>.
- [18] M. Montemurro, A. Catapano, On the effective integration of manufacturability constraints within the multi-scale methodology for designing variable angle-tow laminates, *Composite Structures* 161 (2017) 145 – 159. doi:<https://doi.org/10.1016/j.compstruct.2016.11.018>.
- [19] P. Hao, X. Yuan, H. Liu, B. Wang, C. Liu, D. Yang, S. Zhan, Isogeometric buckling analysis of composite variable-stiffness panels, *Composite Structures* 165 (2017) 192–208.

- [20] Y. Heydarpour, M. Aghdam, A hybrid bézier based multi-step method and differential quadrature for 3d transient response of variable stiffness composite plates, *Composite Structures* 154 (2016) 344 – 359. doi:<https://doi.org/10.1016/j.compstruct.2016.07.060>.
- [21] R. Sevilla, S. Fernández-Méndez, A. Huerta, 3d nurbs-enhanced finite element method (nefem), *International Journal for Numerical Methods in Engineering* 88 (2) (2011) 103–125.
- [22] F. S. Liguori, G. Zucco, A. Madeo, G. Garcea, L. Leonetti, P. M. Weaver, An isogeometric framework for the optimal design of variable stiffness shells undergoing large deformations, *International Journal of Solids and Structures* 210-211 (2021) 18–34. doi:<https://doi.org/10.1016/j.ijsolstr.2020.11.003>.
- [23] S. Daghighi, P. M. Weaver, Three-dimensional effects influencing failure in bend-free, variable stiffness composite pressure vessels, *Composite Structures* 262 (2021) 113346. doi:<https://doi.org/10.1016/j.compstruct.2020.113346>.
- [24] S. Daghighi, M. Rouhi, G. Zucco, P. M. Weaver, Bend-free design of ellipsoids of revolution using variable stiffness composites, *Composite Structures* 233 (2020) 111630. doi:<https://doi.org/10.1016/j.compstruct.2019.111630>.
- [25] A. W. Blom, P. B. Stickler, Z. Gürdal, Optimization of a composite cylinder under bending by tailoring stiffness properties in circumferential direction, *Composites Part B: Engineering* 41 (2) (2010) 157 – 165. doi:<https://doi.org/10.1016/j.compositesb.2009.10.004>.
- [26] M. A. Thomas, S. R. Hallett, P. M. Weaver, Design considerations for variable stiffness, doubly curved composite plates, *Composite Structures* 244 (2020) 112170. doi:<https://doi.org/10.1016/j.compstruct.2020.112170>.
- [27] E. Lemaire, S. Zein, M. Bruyneel, Optimization of composite structures with curved fiber trajectories, *Composite Structures* 131 (2015) 895 – 904. doi:<https://doi.org/10.1016/j.compstruct.2015.06.040>.
- [28] P. Hao, D. Liu, Y. Wang, X. Liu, B. Wang, G. Li, S. Feng, Design of manufacturable fiber path for variable-stiffness panels based on lamination parameters, *Composite Structures* 219 (2019) 158 – 169. doi:<https://doi.org/10.1016/j.compstruct.2019.03.075>.
- [29] T. Vo-Duy, V. Ho-Huu, T. Do-Thi, H. Dang-Trung, T. Nguyen-Thoi, A global numerical approach for lightweight design optimization of laminated composite plates subjected to frequency constraints, *Composite Structures* 159 (2017) 646 – 655. doi:<https://doi.org/10.1016/j.compstruct.2016.09.059>.
- [30] T. Shafighfard, E. Demir, M. Yildiz, Design of fiber-reinforced variable-stiffness composites for different open-hole geometries with fiber continuity and curvature constraints, *Composite Structures* 226 (2019) 111280.

- [31] D. M. Peeters, S. Hesse, M. M. Abdalla, Stacking sequence optimisation of variable stiffness laminates with manufacturing constraints, *Composite Structures* 125 (2015) 596 – 604. doi:<https://doi.org/10.1016/j.compstruct.2015.02.044>.
- [32] X. Niu, T. Yang, Y. Du, Z. Xue, Tensile properties of variable stiffness composite laminates with circular holes based on potential flow functions, *Archive of Applied Mechanics* 86 (9) (2016) 1551–1563.
- [33] P. Hao, C. Liu, X. Yuan, B. Wang, G. Li, T. Zhu, F. Niu, Buckling optimization of variable-stiffness composite panels based on flow field function, *Composite Structures* 181 (2017) 240–255.
- [34] A. Bhatti, Advanced topics in finite element analysis of structures, JOHN WILEY ‘I&’ SONS, INC (2006) 1–577.
- [35] V. B. Hammer, M. Bendsøe, R. Lipton, P. Pedersen, Parametrization in laminate design for optimal compliance, *International Journal of Solids and Structures* 34 (4) (1997) 415–434.
- [36] S. Setoodeh, M. M. Abdalla, Z. Gürdal, Design of variable-stiffness laminates using lamination parameters, *Composites Part B: Engineering* 37 (4-5) (2006) 301–309.
- [37] J. Foldager, N. Olhoff, J. Hansen, A novel procedure forcing convexity of ply angle optimization in composite laminates, in: 7th AIAA/USAF/NASA/ISSMO Symposium on Multidisciplinary Analysis and Optimization, 1998, p. 4817.
- [38] A. W. Blom, M. M. Abdalla, Z. Gürdal, Optimization of course locations in fiber-placed panels for general fiber angle distributions, *Composites Science and Technology* 70 (4) (2010) 564–570. doi:<https://doi.org/10.1016/j.compscitech.2009.12.003>.
- [39] C. G. Diaconu, M. Sato, H. Sekine, Layup optimization of symmetrically laminated thick plates for fundamental frequencies using lamination parameters, *Structural and Multidisciplinary Optimization* 24 (2002) 302–311. doi:10.1007/s00158-002-0241-z.
- [40] R. Anay, D. Miller, A. Tssema, R. Wehbe, P. Ziehl, B. Tatting, Z. Gurdal, R. Harik, A. Kidane, An experimental investigation concerning the effect of afp defects on progressive damage in cfrp coupons, *Composite Structures* 279 (2022) 114725.
- [41] ANSYS® v.19.2 library, (2018).